State Feedback and Proportional-Integral-Derivative Control of a Magnetic Levitation System

Claudia-Adina Bojan-Dragos, Stefan Preitl, Radu-Emil Precup, Stefania Hergane, Edith Georgiana Hughiet, Alexandra-Iulia Szedlak-Stinean
Dept. of Automation and Applied Informatics, Politehnica University of Timisoara, Timisoara, Romania
{claudia.dragos, stefan.preitl, radu.precup, alexandra-iulia.stinean}@upt.ro, stefania.hergane@yahoo.com, hughiet.georgiana@gmail.com

***Abstract*—The paper presents the design of two low-cost control solutions (CSs) for a laboratory equipment, a state feedback CS and a proportional-integral-derivative CS. The two CSs are dedicated to the position control of a ferromagnetic sphere in a Magnetic Levitation System with Two Electromagnets (MLS2EM) and are designed in order to stabilize and to ensure the zero steady-state control error. The nonlinear mathematical model (MM) of the MLS2EM is derived on the basis of the first principles equations with experimentally identified parameters. This unstable and nonlinear MM is next linearized at seven operating points. A system response performance analysis of the best state feedback gain matrix expressed as very good dynamics behavior and settling time is done in order to validate the proposed CSs. Some real-time experimental results are presented in order to validate the proposed control solutions.**

I. Introduction

The "magnetic levitation problem" is a classical automatic control task, used in many practical applications. During the years, classical proportional-integral (PI) or proportional-integral-derivative (PID) and modern control solutions of magnetic levitation systems (MLSs) have been proposed to solve this problem [1]–[9]. For a MLS setup, a linearized controller, developed based on the fuzzy-gain scheduling and sliding mode control strategy – based on the Ackermann's and Utkin's methods – is suggested in [10]. PID-based solutions are presented in [12]–[16] and fuzzy PI and PID control solutions are given in [17], [18] with rather general applicability and comparisons.

This paper proposes the design of a state feedback control solution (SFCS) and of a control solution (CS) based on PID controllers (PID-Cs) in order to stabilize and to ensure the zero steady-state control error by applying the control signal only to the top electromagnet. The control signal applied to the bottom electromagnet is zero; this input can be considered also as an exogenous disturbance.

The paper is organized as follows: the nonlinear model and the linearized mathematical model (LMM) of the laboratory setup are given in Section II. The proposed control solution is next developed in Section III and the experimental results are presented in Section IV and the conclusions are highlighted in Section V.

II. Mathematical Models of MLS2EM

The controlled plant taken into consideration is the complete control laboratory system based on the Magnetic Levitation System with Two Electromagnets (MLS2EM). The MLS2EM laboratory equipment includes both hardware and software components: two electromagnets (EM1 – the upper electromagnet and EM2 – the lower electromagnets), the ferromagnetic sphere, sensors to detect the position of the sphere, computer interface, drivers, power supply unit, connection cables and an acquisition board RT-DAC4 / PCI. When both electromagnets, EM1 and EM2, are used, the control signal applied to EM2 can be used as an additional force leading to Multi Input-Multi Output (MIMO) control systems. This feature is also useful in robust applications. On the other hand, the lower electromagnet, EM2, can be considered as a disturbance input – as an external force excitation. The schematic diagram of the MLS2EM laboratory setup is presented in Fig. 1, where m is the mass of the sphere, F_{em1} and F_{em2} are the electromagnetic forces, and F_g is the gravity force [19].

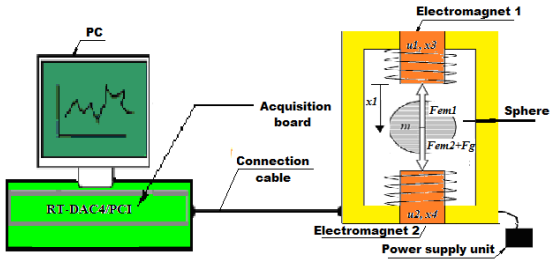

Fig. 1. The MLS2EM laboratory setup.

The nonlinear state-space mathematical model of ML2SEM is [19]

$$\begin{cases} \dot{x}_1 = x_2, \\ \dot{x}_2 = -F_{em1}/m + g + F_{em2}/m, \\ \dot{x}_3 = (k_i u_1 + c_i - x_3)/f_i(x_1), \\ \dot{x}_4 = (k_i u_2 + c_i - x_4)/f_i(x_d - x_1), \\ y = k_m x_1, \end{cases} \quad (1)$$

with the electromagnetic forces, F_{em1} and F_{em2}

$$
\begin{aligned}
F_{em1} &= x_3^2 F_{emP1} \exp(-x_1 / F_{emP2}) / F_{emP2}, \\
F_{em2} &= x_4^2 F_{emP1} \exp(-(x_d - x_1) / F_{emP2}) / F_{emP2}, \\
f_i(x_1) &= f_{iP1} \exp(-x_1 / f_{iP2}) / f_{iP2}, \\
f_i(x_d - x_1) &= f_{iP1} \exp(-(x_d - x_1) / f_{iP2}) / f_{iP2}.
\end{aligned} \qquad (2)
$$

The model (1) corresponds to a strongly unstable fourth-order system, where: $x_1 \in [0, 0.0016]$ – the sphere position, $x_2 \in \Re$ – the sphere speed, x_3, $x_4 \in [0.03884, 2.38]$ – the currents in the top and bottom electromagnets, u_1, $u_2 \in [0.00498, 1]$ – the signals applied to the upper and lower electromagnets, and y – the process (plant) output; the ML2SEM plant includes the actuators and sensors. The parameters of the MLS2EM are presented in Table I. The characteristics of the sphere position sensor, respective of the coil current are shown in Fig. 2 and Fig. 3, respectively. To build the above characteristics it is necessary to measure the position and the current of the electromagnet coil. The electromagnetic {force ⇔ position} and {force ⇔ coil current} diagrams are illustrated in Fig. 4 and Fig. 5, respectively. The nonlinearity $f_i(x_1)$ related to (2) is presented in Fig. 6.

TABLE I.
MLS2EM PARAMETERS

Parameters	Values	Units
m	0.0571	[kg]
g	9.81	[m/s^2]
F_{emP1}	1.7521*10^{-2}	[H]
F_{emP2}	5.8231*10^{-3}	[m]
f_{iP1}	1.4142*10^{-4}	[ms]
f_{iP2}	4.5626*10^{-3}	[m]
k_i	0.0243	[A]
c_i	2.5165	[A]
d	0.09	[m]
D_s	0.06	[m]
x_d	d-D_s	[m]

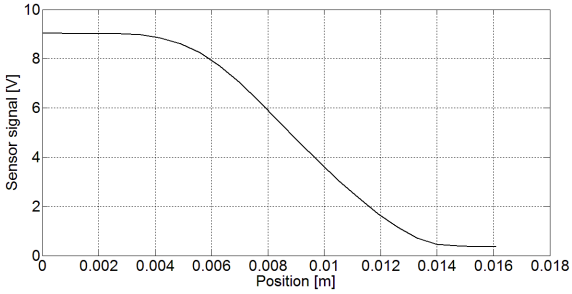

Fig. 2. Characteristics of the sphere position sensor.

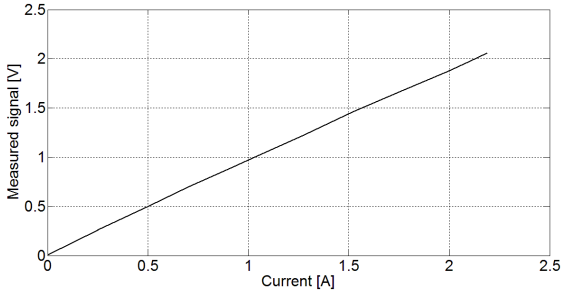

Fig. 3. Characteristics of the coil current sensor.

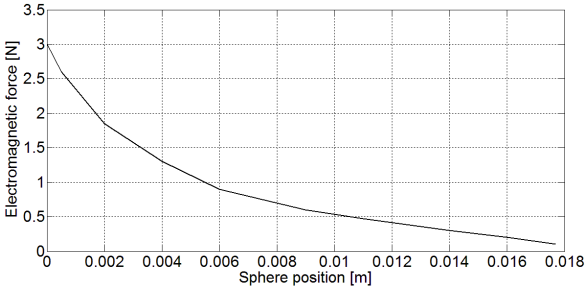

Fig. 4. The electromagnetic force vs. position diagram.

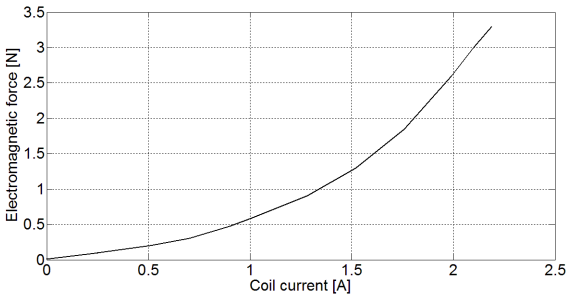

Fig. 5. The electromagnetic force vs. coil current diagram.

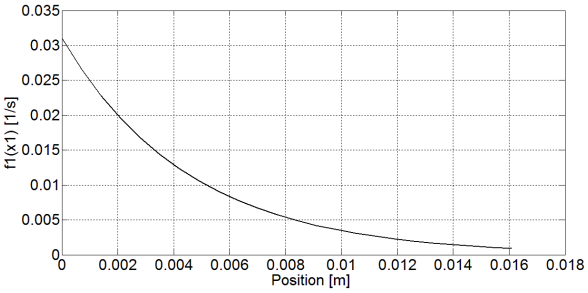

Fig. 6. The nonlinearity $f_i(x_1)$.

Taking into account the particularity of the nonlinearities (continuity and monotony), the structural properties of the process are checked with reference to the state-space model (1) linearized around seven operating points (o.p.s). The following state-space LMMs are obtained:

$$\begin{cases}\Delta\dot{\mathbf{x}}_i = \mathbf{A}_i\,\Delta\mathbf{x}_i + \mathbf{b}_i\,\Delta\mathbf{u}_i \\ \Delta y_i = \mathbf{c}_i^T\Delta\mathbf{x}_i\end{cases},\quad \Delta\mathbf{u}_i = \begin{bmatrix}\Delta u_{1\_i}\\ \Delta u_{2\_i}\end{bmatrix},$$
$$\Delta\mathbf{x}_i = [\Delta x_{1\_i}\quad \Delta x_{2\_i}\quad \Delta x_{3\_i}\quad \Delta x_{4\_i}]^T,$$
$$\Delta y_i = \Delta x_{1\_i},$$
$$\mathbf{A}_i = \begin{bmatrix}0 & 1 & 0 & 0\\ a_{21} & 0 & a_{23} & a_{24}\\ a_{31} & 0 & a_{33} & 0\\ a_{41} & 0 & 0 & a_{44}\end{bmatrix},\quad (3)$$
$$\mathbf{b}_i = [\mathbf{b}_{u_{1\_i}}\quad \mathbf{b}_{u_{2\_i}}] = \begin{bmatrix}0 & 0\\ 0 & 0\\ b_{31} & 0\\ 0 & b_{42}\end{bmatrix},$$
$$\mathbf{c}_i^T = [1\quad 0\quad 0\quad 0].$$

with the matrix parameters

$$a_{21} = \frac{x_{30}^2}{m}\frac{F_{emP1}}{F_{emP2}^2}e^{-\frac{x_{10}}{F_{emP2}}} + \frac{x_{40}^2}{m}\frac{F_{emP1}}{F_{emP2}^2}e^{-\frac{x_d - x_{10}}{F_{emP2}}},$$
$$a_{23} = -\frac{2x_{30}}{m}\frac{F_{emP1}}{F_{emP2}}e^{-\frac{x_{10}}{F_{emP2}}}, a_{24} = \frac{2x_{40}}{m}\frac{F_{emP1}}{F_{emP2}}e^{-\frac{x_d - x_{10}}{F_{emP2}}},$$
$$a_{31} = -(k_i u_1 + c_i - x_{30})\frac{x_{10}}{f_{iP1}}\cdot e^{\frac{x_{10}}{f_{iP1}}},\quad (4)$$
$$a_{33} = -\frac{f_{iP2}}{f_{iP1}}\cdot e^{\frac{x_{10}}{f_{iP2}}}, a_{44} = -\frac{f_{iP2}}{f_{iP1}}\cdot e^{\frac{x_d - x_{10}}{f_{iP2}}},$$
$$a_{41} = -(k_i u_2 + c_i - x_{40})\cdot\frac{x_{10}}{f_{iP1}}\cdot e^{\frac{x_d - x_{10}}{f_{iP2}}},$$
$$b_{31} = k_i\cdot\frac{f_{iP2}}{f_{iP1}}\cdot e^{\frac{x_{10}}{f_{iP2}}}, b_{42} = k_i\cdot\frac{f_{iP2}}{f_{iP1}}\cdot e^{\frac{x_d - x_{10}}{f_{iP2}}}.$$

where $i = \overline{1,7}$ is the index of the operating points $P_i(x_{10\_i}, x_{20\_i}, x_{30\_i}, x_{40\_i})$ detailed in Table II, which were chosen from the middle steady state zone of the sphere position sensor characteristics, shown in Fig. 2 (it is advised to avoid to choosing from extremity of the characteristics, due to instabilities that may occur); $\Delta x_{k\_i} = x_{k\_i} - x_{k0\_i}$, $k = \overline{1,4}, i = \overline{1,7}$, $\Delta u_{k\_i} = u_{k\_i} - u_{k0\_i}$, $k \in \{1,2\}, i = \overline{1,7}$ and $\Delta y_i = y_i - y_{0\_i}$ are the differences of the variables x_{k_i}, u_{k_i} and y_i with respect to the values at the operating point, x_{k0_i}, u_{k0_i} and y_{0_i}, respectively.

The continuity and the monotone variation of the parameters of the plant allow the controllability testing of the model based on

$$\mathbf{Q}_c = [\mathbf{b}_{u_{1\_i}}\quad \mathbf{A}_i\mathbf{b}_{u_{1\_i}}\quad \mathbf{A}_i^2\mathbf{b}_{u_{1\_i}}\quad \mathbf{A}_i^3\mathbf{b}_{u_{1\_i}}\ldots].\quad (5)$$

The controllability test is straightforward. Due to the reducing order of the linear system model from a fourth-order system to a third-order system with the following remaining state variables: the position Δx_{1_i}, the speed Δx_{2_i} and the upper current Δx_{3_i}.

The transfer function (t.f) corresponding to the state-space LMM (3) is

$$H_{P_{i=\overline{1,7}}}(s) = \mathbf{c}_i^T(s\mathbf{I} - \mathbf{A}_i)^{-1}\mathbf{b}_{u_{1\_i}} = \frac{k_i / \prod_{k=\overline{1,3}} p_{k\_i}}{\prod_{k=\overline{1,3}}(s - p_{k\_i})} = \frac{k_{P_i}}{\prod_{k=\overline{1,3}}(1 + T_{k\_i}s)},\quad (6)$$

where $\mathbf{I}$ is the third-order identity matrix and the time constants of the plant are $T_{k\_i} = -1/p_{k\_i}$, $k = \overline{1,3}, i = \overline{1,7}$. The t.f.s $H_{P_{i=\overline{1,7}}}(s)$ for the seven operating points are synthesized in Table II and the plant poles are given in Table III.

TABLE II.
OPERATING POINTS AND TRANSFER FUNCTIONS OF THE PLANT

Operating points $P_i(x_{10\_i}, x_{20\_i}, x_{30\_i}, x_{40\_i})$, $i = \overline{1,7}$		The state variables x_{k0_i}, $k = \overline{1,4}, i = \overline{1,7}$				Control signals		Transfer functions $H_{P_{i=\overline{1,7}}}(s)$
		x_{10_i}	x_{20_i}	x_{30_i}	x_{40_i}	u_{10_i}	u_{20_i}	
(1)	$P_1(x_{10\_1}, x_{20\_1}, x_{30\_1}, x_{40\_1})$	0.0063	0	1.2185	0.039	0.48	0.005	$\frac{0.0241}{(1-0.0148s)(1+0.0148s)(1+0.0078s)}$
(2)	$P_2(x_{10\_2}, x_{20\_2}, x_{30\_2}, x_{40\_2})$	0.007	0	1.145	0.039	0.45	0.005	$\frac{0.0274}{(1-0.0167s)(1+0.0167s)(1+0.0067s)}$
(3)	$P_3(x_{10\_3}, x_{20\_3}, x_{30\_3}, x_{40\_3})$	0.0077	0	1.07	0.039	0.42	0.005	$\frac{0.0274}{(1-0.0190s)(1+0.0190s)(1+0.0057s)}$
(4)	$P_4(x_{10\_4}, x_{20\_4}, x_{30\_4}, x_{40\_4})$	0.0084	0	1	0.039	0.39	0.005	$\frac{0.0293}{(1-0.0216s)(1+0.0216s)(1+0.0049s)}$
(5)	$P_5(x_{10\_5}, x_{20\_5}, x_{30\_5}, x_{40\_5})$	0.009	0	0.9345	0.039	0.36	0.005	$\frac{0.0314}{(1-0.0243s)(1+0.0243s)(1+0.0043s)}$
(6)	$P_6(x_{10\_6}, x_{20\_6}, x_{30\_6}, x_{40\_6})$	0.0098	0	0.89	0.039	0.34	0.005	$\frac{0.0329}{(1-0.0274s)(1+0.0274s)(1+0.0036s)}$
(7)	$P_7(x_{10\_7}, x_{20\_7}, x_{30\_7}, x_{40\_7})$	0.0105	0	0.83	0.039	0.32	0.005	$\frac{0.0353}{(1-0.0312s)(1+0.0312s)(1+0.0031s)}$

III. Control Structures Design

A. Design of the State Feedback Control Solution

Starting with the linearized state-space model (3), the SFCS based on the control system structure presented in Fig. 7, is designed to stabilize the sphere in the MLS2EM. u_1 is the control signal like an external pulse excitation, u_{1x} is the reference input. To compute the state feedback gain matrix $\mathbf{k}_{c\_i}^T = [k_{c1\_i} \;\; k_{c2\_i} \;\; k_{c3\_i}]^T$, $i = \overline{1,7}$, the pole placement method is applied.

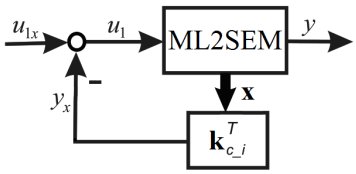

Fig. 7. Block diagram of state feedback control system structure (k_{AS}=1).

Therefore, for each linearized models, with the t.f.s. $H_{P_{i=\overline{1,7}}}(s)$ given in Table II, the closed-loop system poles $p_{k\_i}^*, k = \overline{1,3}, i = \overline{1,7}$ (see Table III) are imposed, which can ensure appropriate state feedback gain matrix to move and keep the sphere at the desired position from the upper electromagnet. Due to the fact that the position is referred in negative values, the expression of the resulted closed-loop t.f.s of SFCS, $H_{SFCS\_i}(s), i = \overline{1,7}$, are

$$\begin{aligned} H_{SFCS\_i}(s) &= H_{x\_i}(s) = \mathbf{c}_i^T (s\mathbf{I} - \mathbf{A}_{x\_i})^{-1}\mathbf{b}_{u_1\_i} = \\ &= \mathbf{c}_i^T [s\mathbf{I} - (\mathbf{A}_i - \mathbf{b}_{u_1\_i}\mathbf{k}_{c\_i}^T k_{AS})]^{-1}\mathbf{b}_{u_1\_i} = \\ &= -k_{x\_i} / \prod_{k=\overline{1,3}} (s - p_{k\_i}^*) = \\ &= -k_{SFCS\_i} / [(1 + T_{1x\_i}s)(1 + 2\zeta_i T_{2x\_i}s + T_{2x\_i}^2 s^2)], \end{aligned} \tag{7}$$

where $k_{SFCS\_i} = k_{x\_i} / \prod_{k=\overline{1,3}} p_{k\_i}^*$.

In order to validate the "best state feedback gain matrix" $\mathbf{k}_{cbest}^T$ which supports the development of the proposed PID solutions, the following experiments were conducted:

- The reference input was set to keep the sphere at 0.007 m from the upper electromagnet.
- Each set of parameter $\mathbf{k}_{c\_i}^T, i = \overline{1,7}$ from Table II was tested on the laboratory setup and the best case was obtained for state feedback gain matrix $\mathbf{k}_{cbest}^T = \mathbf{k}_{c\_5}^T = [66.63 \;\; 1.62 \;\; -0.15]$ in which case the overshoot is $\sigma_{1\_5} = 1.025$, settling time $t_{r\_5} = 1.5$ and the steady-state control error $e_{x\_i,j} = 0.0041$. The best experimental result is illustrated in Section IV in Fig. 9.
- Forwards, the best state feedback gain matrix $\mathbf{k}_{c\_5}^T$ from Table II (dashed) was applied on the linearized model (3), $H_{P_{i=\overline{1,7}}}(s)$, resulting two types of closed-loop t.f.s of the new state feedback control solution (nSFCS) $H_{SFCS\_5,i}(s), i = \overline{1,7}$, with the general expression

$$\begin{aligned} H_{SFCS\_5,i}(s) &= H_{x\_5,i}(s) = \mathbf{c}_i^T (s\mathbf{I} - \mathbf{A}_{x\_5,i})^{-1}\mathbf{b}_{u_1\_i} = \\ &= \mathbf{c}_i^T [s\mathbf{I} - (\mathbf{A}_i - \mathbf{b}_{u_1\_i}\mathbf{k}_{c\_5}^T k_{AS})]^{-1}\mathbf{b}_{u_1\_i} \end{aligned} \tag{8}$$

and the following specific expression obtained after the computation:

$$H_{SFCS\_5,i}(s) = \begin{cases} \dfrac{k_{SFCS\_5,i}}{(1 + T_{1x\_5,i}s)(1 + 2\zeta_{5,i}T_{2x\_5,i}s + T_{2x\_5,i}^2 s^2)}, \\ \quad i = \overline{1,3}, i \in \{6,7\}, \\ \dfrac{k_{SFCS\_5,i}}{(1 + T_{1x\_5,i}s)(1 + T_{2x\_5,i}s)(1 + T_{3x\_5,i}s)}, i \in \{4,5\}. \end{cases} \tag{9}$$

The nSFCS parameters used in the next PID-C obtained with the state feedback gain matrix $\mathbf{k}_{c\_5}^T$ in the row (5) are given in Table IV.

TABLE III.
The Poles of the Plant, the Imposed Poles and the Gain Matrix

O.p.s $P_{i=\overline{1,7}}$	**Plant poles** $p_k^i = -1/T_k^i, k = \overline{1,3}, i = \overline{1,7}$			**Imposed poles** $p_k^{*i}, k = \overline{1,3}, i = \overline{1,7}$			**Gain Matrices** $\mathbf{k}_{c\_i}^T, i = \overline{1,7}$
	p_1^i	p_2^i	p_3^i	p_1^{*j}	p_2^{*j}	p_3^{*j}	
(1)	67.49	-67.49	-128.34	-57.36	-67.55	-128.47	[117.5 1.74 −0.39]
(2)	59.72	-59.72	-149.62	-35.83	-59.72	-149.62	[87.5 1.46 −0.25]
(3)	52.55	-52.55	-174.43	-39.41	-52.56	-174.44	[83.15 1.58 −0.2]
(4)	46.25	-46.25	-203.36	-35.84	-46.25	-203.36	[74.35 1.6 −0.16]
(5)	41.05	-41.05	-231.94	-31.81	-41.05	-231.94	[66.63 1.62 −0.15]
(6)	36.5	-36.52	-276.39	-36.5	-38.33	-276.42	[70.5 1.93 −0.11]
(7)	32.06	-32.06	-322.22	-32.06	-32.38	-337.37	[65.3 2.04 −0.10]

TABLE IV.
THE NSFCS PARAMETERS

O.p.s $P_{i=\overline{1,7}}$	nSFCS parameters				
	$k^i_{SFCS\_5}$	$T^i_{1x\_5}$	$T^i_{2x\_5}$	ζ^i_5	$T^i_{etax\_5}$
(1)	0.084	0.0988	-	0.6	0.0077
(2)	0.065	0.0778	-	0.7	0.0078
(3)	0.054	0.0618	-	0.9	0.0081
(4)	0.046	0.0485	0.0123	-	-
(5)	0.041	0.0314	0.0244	-	-
(6)	0.038	0.0033	-	0.9	0.0308
(7)	0.034	0.0026	-	0.7	0.0332

B. Design of PID Controllers

Due to the fact that the natural SFCS does not contain the *I* component, so it could not ensure the zero steady-state control error, the SFCS, as controlled plant, was included in a cascade control structure (CCS) with PID controller in the outer loop. Depending on the operating points, seven control solutions with PID controllers have been designed using pole-zeros compensation method. The t.f.s of the designed PID controllers extended with a first order lag filter are expressed as [13], [15]–[17]:

$$H_{PID\_5,i}(s)=\begin{cases}\dfrac{k_{c\_5,i}(1+2\zeta_{c\_5,i}T_{c\_5,i}s+T^2_{c\_5,i}s^2)}{s(1+T_{fd\_5,i}s)},\\ i\in\{1,2,3,6,7\}\\ \dfrac{k_{c\_5,i}(1+T_{c1\_5,i}s)(1+T_{c2\_5,i}s)}{s(1+T_{fd\_5,i}s)}, i\in\{4,5\}\end{cases} \tag{10}$$

with the tuning parameters, $k_{c\_5,i}$, $T_{c\_5,i}$ and $T_{fd\_5,i}$

$$k_{c\_5,i}=\begin{cases}1/(2\cdot k_{SFCS\_5,i}\cdot T_{etax\_5,i}), i=\overline{1,3},\\ 0.05/(2\cdot k_{SFCS\_5,i}\cdot T_{\Sigma x\_5,i}), i\in\{4,5\},\\ 0.01/(2\cdot k_{SFCS\_5,i}\cdot T_{1x\_5,i}), i\in\{6,7\},\end{cases}$$

$$T_{c\_5,i}=\begin{cases}T_{1x\_5,i}, i\in\{4,5\},\\ T_{etax\_5,i}, i\in\{1,2,3,6,7\},\end{cases} \tag{11}$$

$$T_{c2\_5_j}=T_{2x\_5,i}, \zeta_{c\_5,i}=\zeta_{5,i}, T_{fd\_5,i}=0.1\cdot T_{1x\_5,i}.$$

Due to the oscillatory regime, the t.f.s coefficients $k_{c\_5,i}$ must be adjusted. The numerical values of PID-C parameters and the system performance indices (overshoot and settling time) are synthesized in Table V.

IV. EXPERIMENTAL RESULTS

The proposed control solutions (SFCS and PID-C) were tested on the nonlinear system setup and validated by real-time experiments. In all cases, the reference input was set to an equivalent of 0.007 m from the upper electromagnet and the control structures responses were tested in 20 sec. The following experimental scenarios were done: (a) real-time experimental results of state feedback control system structure with the best state feedback gain matrix are presented in Fig. 8; (b) real-time experimental results of CCS with PID controller designed at the operating points (3), (5) and (6) are presented in Fig. 9.

The results given in Fig. 9 are better in comparison with those presented in Fig. 8 due to the PID-C that ensures the zero steady-state control error and the reference input is well tracked. Due to the nonlinearities of the plant and the presents of the complex conjugated poles in the cases (1)-(3) and (6), (7) some oscillations occur at the beginning of transience responses and during the real-time experiments.

TABLE V.
PID-CS PARAMETERS

O.p.s $P_{i=\overline{1,7}}$	PID-CS tuning parameters		PID-CS performance indices	
	$k_{c\_5,i}$	$T_{fd\_5,i}$	$t_{r\_5,i}$	$\sigma_{1\_5,i}$
(1)	60.65	0.009	4,25	0,24
(2)	98.23	0.008	4,25	0,24
(3)	150.83	0.006	4,5	0,24
(4)	89.88	0.005	5,0	0,23
(5)	28.67	0.003	4,0	0,23
(6)	40.98	0.003	3,5	0,24
(7)	111.24	0.003	4,0	0,24

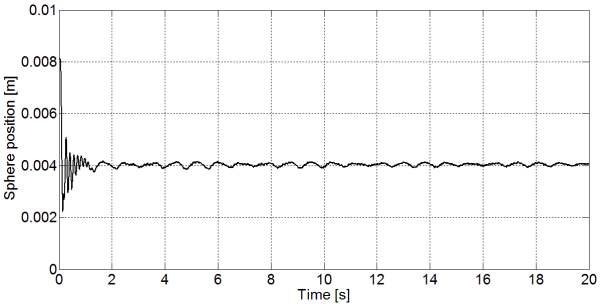

Fig. 8. Real-time experimental results of state feedback control system structure with the best state feedback gain matrix, $\underline{\mathbf{k}}^T_{cbest}$.

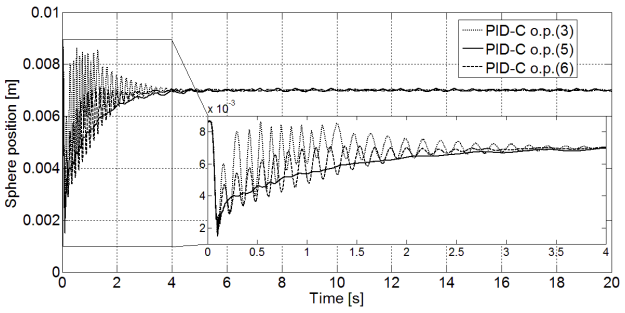

Fig. 9. Real-time experimental results of CCS with PID-C designed for the operating points (3), (5) and (6).

V. CONCLUSION

The paper presented three control solutions dedicated to the position control of magnetic levitation system with two electromagnets. The nonlinear model of the MLS2EM was linearized around seven operating points.

A state feedback control structure was designed and the best state feedback gain matrix was found in order to

stabilize the system. Because the SFCS does not ensure the zero steady state control error, seven PID controllers were designed. The proposed control structures were tested on the nonlinear model, accepting the main values of the parameters given in [19]. The real-time experimental results prove that the proposed PID-C control structures guarantee the improvement of control system performance regarding to step modifications of reference input; they ensure the zero steady-state control error, small settling time and small overshoot.

Future research will be focused on the design of the control systems with PI(D) fuzzy gain-scheduling controllers, Takagi-Sugeno fuzzy controllers and combined control solutions which can ensure the zero steady-state control error, small settling time and small overshoot. Different modeling, optimization and modeling methodologies will be used [20]–[30].

ACKNOWLEDGMENT

This work was supported by grants from the Partnerships in priority areas – PN II program of the Romanian Ministry of Education and Research (MEdC) – the Executive Agency for Higher Education, Research, Development and Innovation Funding (UEFISCDI), project numbers PN-II-PT-PCCA-2013-4-0544 and PN-II-PT-PCCA-2013-4-0070.

REFERENCES

[1] E. Shameli, M. B. Khamesee, and J. P. Huissoon, "Nonlinear controller design for a magnetic levitation device," *Microsystem Technologies*, vol. 13, pp. 831–835, May 2007.

[2] B. Wang, G.-P. Liu, and D. Rees, "Networked predictive control of magnetic levitation system," in *Proc. 2009 IEEE International Conference on Systems, Man and Cybernetics*, San Antonio, TX, USA, 2009, pp. 4100–4105.

[3] S. An, Y. Ma, and Z. Cao, "Applying simple adaptive control to magnetic levitation system," in *Proc. 2nd International Conference on Intelligent Computation Technology and Automation*, Changsha, Hunan, China, 2009, vol. 1, pp. 746–749.

[4] H. Wu and Y. Hu, "Study on fuzzy control algorithm for magnetic levitated platform," in *Proc. 2009 International Conference on Measuring Technology and Mechatronics Automation*, Hunan, China, 2009, vol. 2, pp. 598–601.

[5] J. Zietkiewicz, "Constrained predictive control of a levitation system," in *Proc. 16th Intl. Conf. on Methods and Models in Automation and Robot.*, Miedzyzdroje, Poland, 2011, pp. 278–283.

[6] L. Seban, N. Sahoo, and B. K. Roy, "Multiple model based predictive control of magnetic levitation system," in *Proc. 2014 Annual IEEE India Conference*, Pune, India, 2014, pp. 1–5.

[7] C. A. Camasca, A. K. Swain, and N. D. Patel, "Bit-stream based model predictive controller for a magnetic levitation system," in *Proc. 2011 IEEE Region 10 Conference*, Bali, Indonesia, 2011, pp. 1055–1059.

[8] C.-A. Dragos, S. Preitl, R.-E. Precup, R.-G. Bulzan, C. Pozna, and J. K. Tar, "Takagi-Sugeno fuzzy controller for a magnetic levitation system laboratory equipment," in *Proc. International Joint Conferences on Computational Cybernetics and Technical Informatics*, Timisoara, Romania, 2010, pp. 55–60.

[9] S. Chauhan and M. J. Nigam, "Model predictive controller design and perturbation study for magnetic levitation system," in *Proc. 2014 IEEE Recent Advances in Engineering and Computational Sciences*, Chandigarh, India, 2014, pp. 1–6.

[10] M. Lashin, A. T. Elgammal, A. Ramadan, A. A. Abouelsoud, S. F. M. Assal, and A. Abo-Ismail, "Fuzzy-based gain scheduling of exact feedforward linearization control and SMC for magnetic ball levitation system: A comparative study," in *Proc. 2014 IEEE International Conference on Automation, Quality and Testing, Robotics*, Cluj-Napoca, Romania, 2014, pp. 1–6.

[11] A. Sakalli, T. Kumbasar, E. Yesil, and H. Hagras, "Analysis of the performances of type-1, self-tuning type-1 and interval type-2 fuzzy PID controllers on the magnetic levitation system," in *Proc. 2014 IEEE International Conference on Fuzzy Systems*, Beijing, China, 2014, pp. 1859–1866.

[12] P. Kallakuri, L. H. Keel, and S. P. Bhattacharyya, "Data based design of PID controllers for a magnetic levitation experiment," in *Proc. 18th IFAC World Congress*, Milano, Italy, 2011, pp. 10231–10236.

[13] E. V. Kumar and J. Jerome, "LQR based optimal tuning of PID controller for trajectory tracking of magnetic levitation system," in *Proc. International Conference on Design and Manufacturing*, Chennai, India, 2013, vol. 64, pp. 254–264.

[14] A. Ghosh, T. R. Krishnan, P. Tejaswy, A. Mandal, J. K. Pradhan, and S. Ranasingh,, "Design and implementation of a 2-DOF PID compensation for magnetic levitation systems," *ISA Trans.*, vol. 53, pp. 1216–1222, July 2014.

[15] Pallav, S. K. Pandey, and V. Laxmi, "PID control of magnetic levitation system based on derivative filter," in *Proc. 2014 Annual International Conference on Emerging Research Areas: Magnetics, Machines and Drives*, Kottayam, India, 2014, pp. 1–5.

[16] M. Cetin and S. Iplikci, "A novel auto-tuning PID control mechanism for nonlinear systems," *ISA Trans.*, vol. 58, pp. 292–308, Sep. 2015.

[17] R.-E. Precup, R.-C. David, E. M. Petriu, S. Preitl, and M.-B. Radac, "Gravitational search algorithms in fuzzy control systems tuning," in *Proc. 18th IFAC World Congress*, Milano, Italy, 2011, pp. 13624–13629.

[18] S. Yadav, S. K. Verma, and S. K. Nagar, "Optimized PID controller for magnetic levitation system," in *Proc. 4th IFAC Conference on Advances in Control and Optimization of Dynamical Systems*, Tiruchirappalli, India, 2016, pp. 778–782.

[19] Inteco Ltd, *Magnetic Levitation System 2EM (MLS2EM), User's Manual (Laboratory Set)*. Krakow, Poland: Inteco Ltd., 2008.

[20] S. Preitl and R.-E. Precup, "On the algorithmic design of a class of control systems based on providing the symmetry of open-loop Bode plots," *Sci. Bull. UPT Trans. Autom. Control Comp. Sci.*, vol. 41 (55), no. 2, pp. 47–55, Dec. 1996.

[21] I. Škrjanc and S. Blažič, "Predictive functional control based on fuzzy model: design and stability study," *J. Intell. Robot. Syst.*, vol. 43, pp. 283–299, Aug. 2005.

[22] F. G. Filip, "Decision support and control for large-scale complex systems," *Ann. Rev. Control*, vol. 32, pp. 61–70, Apr. 2008.

[23] L. Horváth and I. J. Rudas, "Intelligent human-computer communication of engineers at extended companies," *J. Adv. Comput. Intell. Intell. Informat.*, vol. 10, pp. 510–516, May 2006.

[24] A. Gajate, R. E. Haber, P. I. Vega, and J. R. Alique, "A transductive neuro-fuzzy controller: Application to a drilling process," *IEEE Trans. Neural Netw.*, vol. 21, pp. 1158–1167, Jul. 2010.

[25] J. Vaščák, "Adaptation of fuzzy cognitive maps by migration algorithms," *Kybernetes*, vol. 41, pp. 429–443, Mar. 2012.

[26] R.-E. Precup, R.-C. David, E. M. Petriu, S. Preitl, and M.-B. Radac, "Fuzzy logic-based adaptive gravitational search algorithm for optimal tuning of fuzzy controlled servo systems," *IET Control Theory Appl.*, vol. 7, pp. 99–107, Jan. 2013.

[27] R.-E. Precup, M.-B. Radac, M. L. Tomescu, E. M. Petriu, and S. Preitl, "Stable and convergent iterative feedback tuning of fuzzy controllers for discrete-time SISO systems," *Expert Syst. Appl.*, vol. 40, pp. 188–199, Jan. 2013.

[28] Z. C. Johanyák, "Fuzzy modeling of thermoplastic composites' melt volume rate," *Comput. Informat.*, vol. 32, pp. 845–857, Dec. 2013.

[29] N. Tomin, A. Zhukov, D. Sidorov, V. Kurbatsky, D. Panasetsky, and V. Spiryaev, "Random forest based model for preventing large-scale emergencies in power systems," *Int. J. Artif. Intell.*, vol. 13, no. 1, pp. 211–228, Oct. 2015.

[30] H.-Y. Xu and R. Vilanova, "PI and fuzzy control for P-removal in wastewater treatment plant," *Int. J. Comput. Commun. Control*, vol. 10, pp. 936–951, Dec. 2015.